ACS SENSORS

pubs.acs.org/acssensors Article

Trapping and Detection of Single Viruses in an Optofluidic Chip

Yuzhi Shi,* Kim Truc Nguyen, Lip Ket Chin, Zhenyu Li, Limin Xiao, Hong Cai, Ruozhen Yu,* Wei Huang, Shilun Feng, Peng Huat Yap, Jingquan Liu,* Yi Zhang,* and Ai Qun Liu*

Cite This: https://doi.org/10.1021/acssensors.1c01350 Read Online

ACCESS | Metrics & More | Article Recommendations

ABSTRACT: Accurate single virus detection is critical for disease diagnosis and early prevention, especially in view of current pandemics. Numerous detection methods have been proposed with the single virus sensitivity, including the optical approaches and immunoassays. However, few of them hitherto have the capability of both trapping and detection of single viruses in the microchannel. Here, we report an optofluidic potential well array to trap nanoparticles stably in the flow stream. The nanoparticle is bound with single viruses and fluorescence quantum dots through an immunolabeling protocol. Single viruses can be swiftly captured in the microchannel by optical forces and imaged by a camera. The number of viruses in solution and on each particle can be quantified via image processing. Our method can trap and detect single viruses in the 1 mL serum or water in 2 h, paving an avenue for the advanced, fast, and accurate clinical diagnosis, as well as the study of virus infectivity, mutation, drug inhibition, etc.

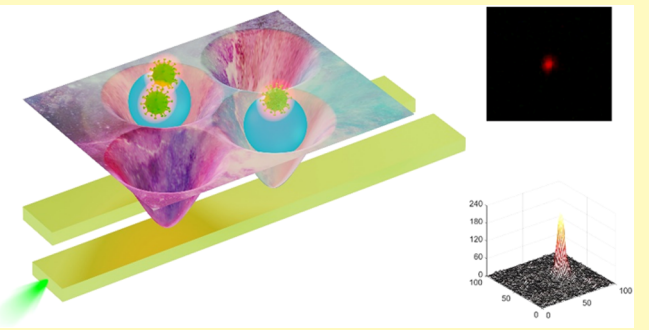

KEYWORDS: *optical trapping, single virus detection, virus quantification, silicon photonics, immunolabeling protocol, near-field manipulation*

Viral pandemics are considered among the world's most critical crises facing mankind, along with energy and water sustainability.[1−3] With increasing urbanization and global travel, the progression from local outbreak to a worldwide pandemic is faster and more probable. From an economic perspective, disease outbreaks are costly to society, especially for global cities.[4] When severe acute respiratory syndrome (SARS) finally waned after more than 100 days, 774 deaths worldwide were counted by the WHO in a geographical area spanning 29 countries in 2003.[5] Most outbreaks and many emerging infectious diseases are viral, including avian influenza (H5N1, H7N9), dengue, and other infections from animals, such as Ebola in monkeys, Zika in mosquitoes, and Nipah in pigs.[6−8] The outbreak of the coronavirus disease-19 (COVID-19) pandemic has caused millions of fatalities and imposed a severe impact on our daily lives globally.[9−11] More severely, the development of detecting methods and vaccines may be compromised by the rapid mutation of viruses.[9,12,13] To counter these viruses, scientists are deploying new tools to identify viruses as well as classical public health measures of quarantine and isolation to retard the spread of epidemics.[6,14−19] However, effective broad-spectrum antiviral therapies are relatively lacking, compared to advances made for bacteria.

Current methods for viral isolation and characterization have not changed significantly for half a century.[20] They are still highly manual and time-consuming, requiring costly bioconta-minant facilities. They involve many steps: purification from cell debris and bacteria; enrichment into a small volume; culture in live host cells; indirect detection of effects on host cell infection (cytopathic effects); and quantification by dilutional titration, further propagation, and characterization. While major advances in new molecular diagnostic techniques have been made, critical challenges remain in virus trapping and sorting to achieve efficient purification and enrichment.[19,21−25] One big challenge lies in the nature of the viruses being small, mostly on the nanoscale ranging from 40 to 300 nm. Up to now, there exists a neither robust nor commercially scalable technique for effective manipulation, sorting, and characterization of individual intact viruses.

Recently, researchers have developed a variety of methods for single virus detection due to low natural concentration levels of the pathogens in the early stage of the disease. Examples include the spectral shift of a whispering-gallery mode[2] and electrical detection for single influenza A virus,[26] cantilever detection of single vaccinia virus,[27] multimode

Received: June 26, 2021

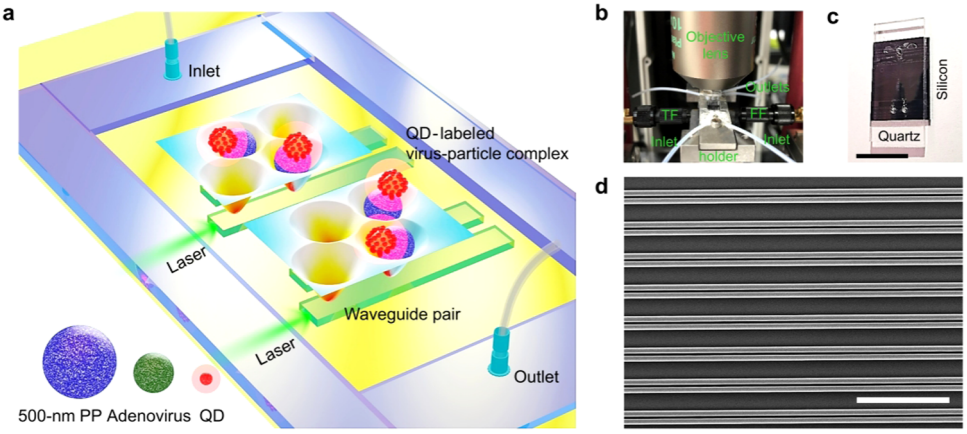

Figure 1. Optical detection of single viruses in an optofluidic chip. (a) Virus bound with the 500 nm polystyrene nanoparticle. The virus−particle complex is also linked with the fluorescence quantum dots. The single viruses can be visualized by observing the fluorescence from the quantum dots. PP: polystyrene nanoparticle. QD: quantum dot. (b) Optical detection system. Light is coupled into the chip using a tapered fiber. Laser power is measured using a flat-end fiber. TF: tapered fiber; FF: flat-end fiber. (c) Photograph of the optofluidic chip. The silicon chip is bound with the glass chip with a 1 μm PMDS layer. The holes are drilled for the inlet and outlet. Scale bar equals 1 cm. (d) SEM image of the nanowaveguide-pair array. The width and the depth of the nanowaveguide are 350 and 220 nm, respectively. The gap between two nanowaveguides and two waveguide pairs are 200 nm and 1 μm, respectively. Scale bar equals 5 μm.

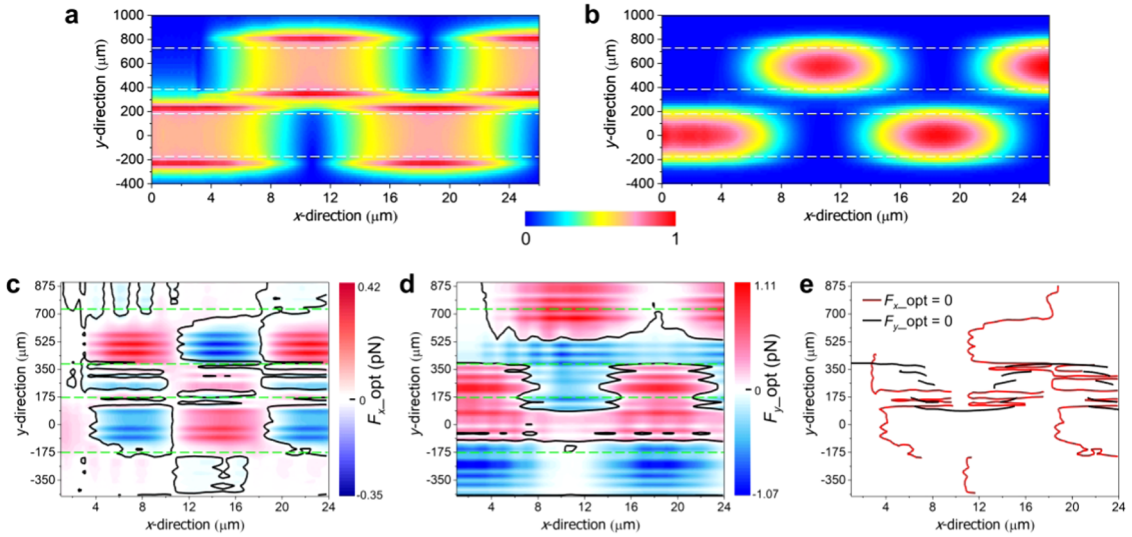

Figure 2. Analysis of optical forces on the 500 nm polystyrene nanoparticles. (a) Electric and (b) intensity field distributions. Optical forces in the (c) x- and (d) y-directions. (e) Determination of optical trapping positions from the intersections of contours with $F_x = 0$ and $F_y = 0$. Red and black contours are stable positions in the x- and y-directions, respectively. The laser powers in (c)−(e) are 10 mW.

interference waveguide for HIN1 and H3N2 viruses,[28,29] differential optical heterodyne detection of HIV virus,[30] Young interferometer sensor for HSV-1 virus,[14] immunolabeling fluorescence imaging of HCMV virus,[31] optical methods and immunoassays for Covid-19,[6,7,12,32] etc. Although most of those methods detect single viruses, there remains a great challenge to simultaneously trap them in the flow stream.[33] Here, we develop an optofluidic chip with a nanowaveguide-pair array, which generates lots of potential wells to trap nanoparticles. The single viruses can be bound with the nanoparticles and fluorescence quantum dots to enable the trapping and detection using an immunolabeling protocol. The number of viruses linked to the particle and the total quantity of viruses in solution can be detected directly by the analysis of the intensities of fluorescence images. Our method is fast and accurate and allows the trapping of single viruses, which consumes very little volume of sample in picoliters and has great potential in the clinical diagnosis.

RESULTS AND DISCUSSION

Design and Working Principle for Single Virus Trapping and Detection. The optofluidic potential well array can capture arbitrary nanoparticles flowing around, as shown in Figure 1. Using the immunolabeling protocol, the single adenovirus is bound with the nanoparticles to experience large optical forces for the trapping in potential wells. The fluorescence quantum dots are labeled to the virus so that the virus can be visualized easily. Light is coupled into the chip using a tapered fiber (Figure 1b) and split into the waveguide pairs using the beam splitter fabricated onto the silicon photonic chip.[34] The coupling of light between two adjacent nanowaveguides (Figure 1d) generates a lot of hotspots, which create potential wells and exert strong optical gradient forces to

https://doi.org/10.1021/acssensors.1c01350
ACS Sens. XXXX, XXX, XXX−XXX

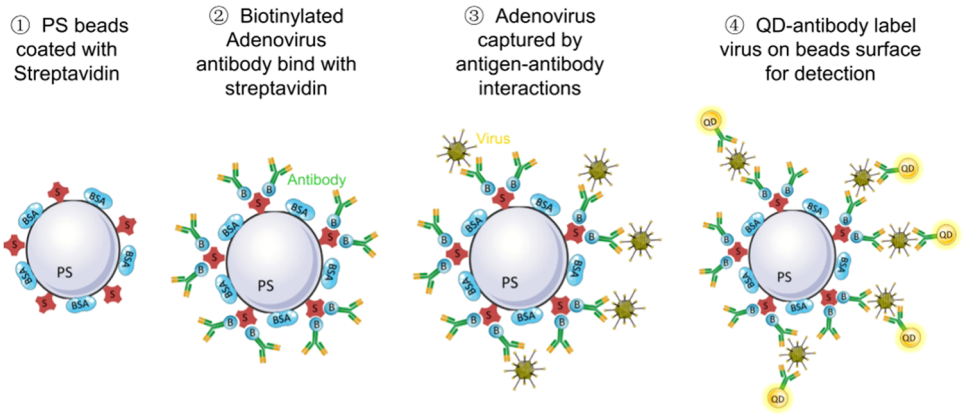

Figure 3. Protocol of immunolabeling of virus, particle, and quantum dots. S and B denote the streptavidin and biotin, respectively.

attract nanoparticles inside. Those coupled potential wells can be used for the sorting of particles with different sizes[34] and shapes.[25] The virus−particle complex is injected into the microchannel with a width of 100 μm and a depth of 1.5 μm. This shallow channel ensures that every complex experiences a strong optical force from the evanescence wave (in a range of a few hundred nanometers) to attract them into the potential wells on the surface of the nanowaveguide.

Analysis of Optical Forces on 500 nm Nanoparticles. Since the width of the nanowaveguide is only 350 nm and the gap between the two nanowaveguides is 200 nm, light has a prominent leakage of electric field on the edge of the nanowaveguide, as shown in Figure 2a, while the intensity of light is still confined inside the nanowaveguide, as shown in Figure 2b. The leakage of the electric field has a strong effect on the distribution of the optical forces because of the polarization of nanoparticles inside the electric field. The simulations of optical forces on a 500 nm polystyrene nanoparticle in the x- and y-directions are shown in Figure 2c,d, respectively. The negative values of F_x at the beginning of the lower nanowaveguide indicate the stronger optical gradient force than the scattering force. And the strong optical gradient force in the y-direction moves the nanoparticle to the two edges of the nanowaveguide. Therefore, the intersection of F_x and F_y determines the stable trapping position, as shown in Figure 2e. The coupling of light from a lower to higher waveguide generates a stable trapping position. It is worth noting that more stable trapping positions will emerge due to the optical binding when one particle is trapped in this position.[25,35] The simulation of the optical forces uses the Minkowski stress tensor conducted in commercial software Lumerical.[25,35−37]

Immunolabeling Protocol, Detection Process Flow, and Experimental Trapping of Virus−Particle Complexes. The adenovirus itself is too small to be trapped because of the small optical forces from the small size (90−100 nm). To trap a variety of single viruses on the surface of the nanowaveguide, we perform the immunolabeling protocol to label the single virus with 500 nm polystyrene nanoparticles (Bangs Laboratories) and fluorescence quantum dots (Thermo Fisher Scientific), as shown in Figure 3. First, a layer of streptavidin is coated to the surface of nanoparticles. Second, the biotinylated adenovirus antibody (Thermo Fisher Scientific) is bound with the streptavidin by the streptavidin−biotin binding. Third, the adenovirus antibody-linked particle captures the adenovirus (Bio-REV) in solution. Finally, the virus−particle conjugation is bound with the antibody-labeled quantum dots, which has a fluorescence excitation from 300 to 500 nm and an emission peak at 625 nm. After binding, the solution with the virus−particle complex is then injected into the optofluidic chip using a syringe pump (SPM 200C, SIMTech, Singapore). The optofluidic chip is the same as our previous chip used for the shape-selective sorting of label-free bacteria.[25] The depth of the microchannel is 1.5 μm to facilitate the trapping of particles in the evanescence wave with the penetration depth of a few hundred nanometers.

Since the samples with viruses may have been mixed with other bigger bioparticles and debris that may influence the detection and clog the shallow microchannel, the first step of the detection process is to filter out big objects using a 200 nm syringe filter. The filter only allows bioparticles smaller than 200 nm, such as the adenovirus with sizes around 90−100 nm, to pass.[38] The adenoviruses after filtration are then labeled with the 500 nm nanoparticles and fluorescence quantum dots using the immunolabeling protocol. The fluorescence viruses are then suspended in the 1 mL solution. Such a large volume takes a very long time to detect since the flow rate in the nano-optofluidic chip is only ∼90 nL/min. To boost the detection time, the 1 mL solution is concentrated to 10 μL using the centrifugal machine. The solution can now be injected into the nano-optofluidic chip for detection in 2 h.

As shown in Figure 4a, the quantity of the trapped virus−particle complex is increased linearly with time until a plateau is reached (∼130), which means that the region of the waveguide array is full of complexes, and no more complexes can be further trapped unless the previously trapped complexes

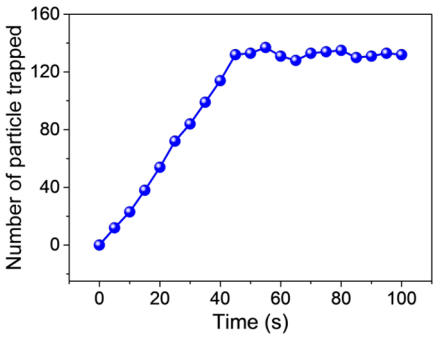

Figure 4. Quantity of virus-particle complexes trapped with time. The laser power is 1 mW.

https://doi.org/10.1021/acssensors.1c01350
ACS Sens. XXXX, XXX, XXX−XXX

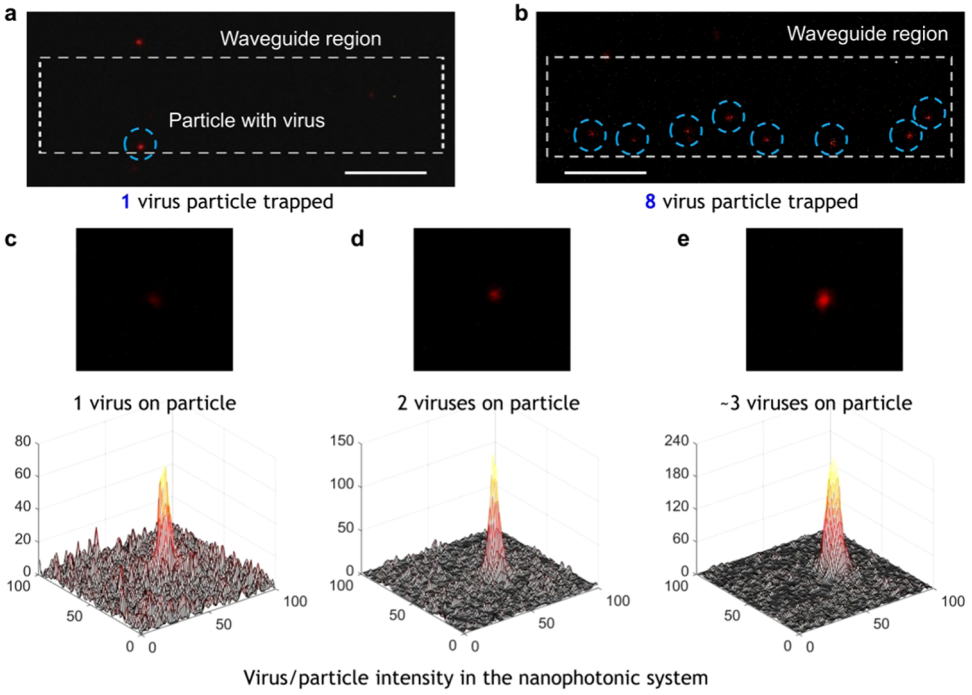

Figure 5. Trapping and imaging of the fluorescence virus−particle complex. Trapping of (a) a single and (b) eight virus−particle complexes. Scale bars in (a) and (b) equal 20 μm. Fluorescence intensities of the virus−particle complex with (c) one, (d) two, and (e) probably three viruses on one particle.

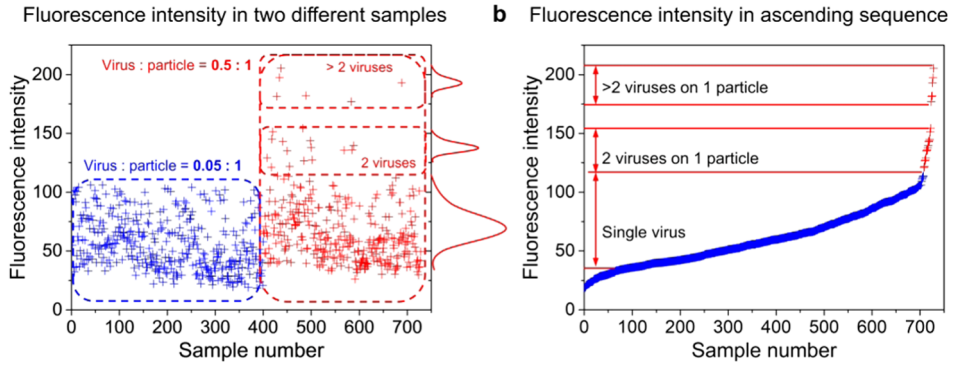

Figure 6. Fluorescence analysis of the trapped virus−particle complex. (a) Fluorescence intensities of the complex come from two batches of samples with the ratio of virus−particle in 0.05 and 0.5. (b) Plot of fluorescence intensities in an ascending sequence. The intensities will have apparent leaps when the number of viruses on one particle increases.

are released from the 16-nanowaveguide-pair chip. Increasing the number of nanowaveguide pairs or expanding the width of the microchannel can significantly expand the trapping space and increase the trapping capability. The trapping efficiency, defined as the trapping number/all complexes flowing to the area, increases with the laser power. The trapping efficiency reaches >95% when the measured output laser power P is 0.5 mW. It continues to reach ∼100% when P is further increased to 1 mW. When $P \leq 0.4$ mW, the depth of the potential well for each hotpot is unable to trap the complex for a long time, and the optical gradient force may not be able to pull the complex from the flow stream to the surface of nanowaveguides, resulting in a lower trapping efficiency, e.g., <50%.

Fluorescence Analysis of Trapped Virus−Particle Complexes. The experimental demonstration of trapping of the single virus−particle complexes is shown in Figure 5. A single complex or eight complexes can be trapped easily on the surface of the nanowaveguide, as shown in Figure 5a,b, respectively. The image of the complex can then be captured by the charge-coupled device (CCD) due to the labeled fluorescence quantum dot, as shown in Figure 5c−e. Since the virus is mixed with saturated quantum dots, the number of quantum dots on each virus is identical or very close, which means that the fluorescence intensity of each virus is very close. Therefore, the intensity of the fluorescence spot increases with the number of viruses on the particle. The intensity is obtained using MATLAB by processing each captured image. The measured fluorescence intensities of one, two, and probably three viruses on one particle are ∼70, 140, and 210, as shown in Figure 5c−e, respectively. The three viruses are not definite as there is little possibility that four viruses with dim fluorescence are conjugates to reach the same intensity, 210. The intensity increases relatively linearly with the virus number per particle. To characterize the fluorescence intensity on different numbers of viruses on one particle, we first control the ratio of virus and particle to 0.05 to make sure that only

https://doi.org/10.1021/acssensors.1c01350
ACS Sens. XXXX, XXX, XXX−XXX

one virus is, in a very high probability, attached to one particle, as shown in Figure 6a. The intensity of a single virus ranges from 20 to 100. The range of intensity comes from the deviation of quantum dot brightness and quantity and dynamic movement (moving higher or lower) of the virus−particle complex on the surface of nanowaveguides. When the ratio of virus and particle increases to 0.5, as shown in the red dots in Figure 6a, the particle will have more chances to be linked with two or more viruses, which will also result in the abrupt increase of the intensity. The range of intensity with one virus for a ratio of 0.5 is the same as that of 0.05. The two additional regions with higher intensities represent the two or more viruses on one particle, which can also be corroborated by the plot of fluorescence intensity in an ascending sequence, as shown in Figure 6b. Very few virus conjugations with intensities higher than 225 are manually omitted as we only care about the low number of viruses on one particle. It is worth noting that the virus concentration in the practical biological medium is not very high, especially in the early stage of the disease. The particle concentration can be changed almost arbitrarily depending on the special requirement. When the virus−particle ratio is too high, e.g., 10:1, the range of virus numbers in one particle could be very broad. In that case, the quantification of the virus number will be very complex and difficult because of the overlap of fluorescence intensities from different virus numbers. Therefore, we choose a low virus−particle ratio (0.05 and 0.5) to better detect and quantify the viruses and to better mimic the practical biological model.

CONCLUSIONS

In summary, single viruses can be easily detected and counted in the optofluidic chip simply by measuring the intensity of the trapped virus−particle complex using an immunolabeling protocol. The intensity of the virus−particle complex is bright enough to be seen in visual or captured by CCD. The intensity increases linearly with the number of viruses attached to one particle, which can be easily processed using the MATLAB code. More importantly, single viruses can also be trapped with 500 nm polystyrene nanoparticles in optical potential wells in the microchannel. The trapping efficiency can reach ∼100% when the measured output laser power is ≥0.5 mW. The trapping of single viruses may facilitate future on-chip pathology diagnosis, virus isolation, and annihilation. It also has great potential in the early detection of diseases when the virus quantity is very small by directly trapping and isolating individual viruses on a chip to study the virus infectivity, mutation, and drug inhibition, as well as being promising to tackle Covid-19. Our study provides a novel way to simultaneous trapping and detection of single viruses in the microchannel, which could inspire future efforts in designing multifunctional particle manipulation and biodetection optofluidic chips.

AUTHOR INFORMATION

Corresponding Authors

Yuzhi Shi − *National Key Laboratory of Science and Technology on Micro/Nano Fabrication, Department of Micro/Nano Electronics, Shanghai Jiao Tong University, Shanghai 200240, China; School of Electrical and Electronic Engineering, Nanyang Technological University, 639798, Singapore;* orcid.org/0000-0002-9041-0462; Email: yuzhi.shi@sjtu.edu.cn

Ruozhen Yu − *Chinese Research Academy of Environmental Science, Beijing 100012, China*; Email: 1323795860@qq.com

Jingquan Liu − *National Key Laboratory of Science and Technology on Micro/Nano Fabrication, Department of Micro/Nano Electronics, Shanghai Jiao Tong University, Shanghai 200240, China;* orcid.org/0000-0003-4140-1516; Email: jqliu@sjtu.edu.cn

Yi Zhang − *School of Mechanical and Aerospace Engineering, Nanyang Technological University, 639798, Singapore*; Email: yi_zhang@ntu.edu.sg

Ai Qun Liu − *School of Electrical and Electronic Engineering, Nanyang Technological University, 639798, Singapore;* orcid.org/0000-0002-0126-5778; Email: eaqliu@ntu.edu.sg

Authors

Kim Truc Nguyen − *School of Electrical and Electronic Engineering, Nanyang Technological University, 639798, Singapore*

Lip Ket Chin − *School of Electrical and Electronic Engineering, Nanyang Technological University, 639798, Singapore*

Zhenyu Li − *School of Electrical and Electronic Engineering, Nanyang Technological University, 639798, Singapore*

Limin Xiao − *Advanced Fiber Devices and Systems Group, Key Laboratory of Micro and Nano Photonic Structures (MoE), Key Laboratory for Information Science of Electromagnetic Waves (MoE), Shanghai Engineering Research Center of Ultra-Precision Optical Manufacturing, School of Information Science and Technology, Fudan University, Shanghai 200433, China;* orcid.org/0000-0002-8791-3456

Hong Cai − *Institute of Microelectronics, A*STAR (Agency for Science, Technology and Research), 138634, Singapore*

Wei Huang − *Key Laboratory of Multifunctional Nanomaterials and Smart Systems, Suzhou Institute of Nano-Tech and Nano-Bionics (SINANO), Chinese Academy of Sciences (CAS), Suzhou 215123, China*

Shilun Feng − *School of Electrical and Electronic Engineering, Nanyang Technological University, 639798, Singapore;* orcid.org/0000-0002-2560-2417

Peng Huat Yap − *Lee Kong Chian School of Medicine, Nanyang Technological University, 308232, Singapore*

Complete contact information is available at: https://pubs.acs.org/10.1021/acssensors.1c01350

Notes

The authors declare no competing financial interest.

ACKNOWLEDGMENTS

This work was supported by the Singapore National Research Foundation under the Competitive Research Program (NRFCRP13-2014-01), and the Singapore Ministry of Education (MOE) Tier 3 grant (MOE2017-T3-1-001).

REFERENCES

(1) Baize, S.; Pannetier, D.; Oestereich, L.; Rieger, T.; Koivogui, L.; Magassouba, N. F.; Soropogui, B.; Sow, M. S.; Keïta, S.; De Clerck, H.; et al. Emergence of Zaire Ebola virus disease in Guinea. *N. Engl. J. Med.* **2014**, *371*, 1418−1425.

(2) Vollmer, F.; Arnold, S.; Keng, D. Single virus detection from the reactive shift of a whispering-gallery mode. *Proc. Natl. Acad. Sci. U.S.A.* **2008**, *105*, 20701−20704.

https://doi.org/10.1021/acssensors.1c01350
ACS Sens. XXXX, XXX, XXX−XXX

(3) Chun, T.-W.; Stuyver, L.; Mizell, S. B.; Ehler, L. A.; Mican, J. A. M.; Baseler, M.; Lloyd, A. L.; Nowak, M. A.; Fauci, A. S. Presence of an inducible HIV-1 latent reservoir during highly active antiretroviral therapy. *Proc. Natl. Acad. Sci. U.S.A.* **1997**, *94*, 13193−13197.
(4) Holtkamp, D. J.; Kliebenstein, J. B.; Neumann, E.; Zimmerman, J. J.; Rotto, H.; Yoder, T. K.; Wang, C.; Yeske, P.; Mowrer, C. L.; Haley, C. A. Assessment of the economic impact of porcine reproductive and respiratory syndrome virus on United States pork producers. *J. Swine Health Prod.* **2013**, *21*, 72.
(5) Stadler, K.; Masignani, V.; Eickmann, M.; Becker, S.; Abrignani, S.; Klenk, H.-D.; Rappuoli, R. SARS—beginning to understand a new virus. *Nat. Rev. Microbiol.* **2003**, *1*, 209.
(6) Shi, Y.; Li, Z.; Liu, P. Y.; Nguyen, B. T. T.; Wu, W.; Zhao, Q.; Chin, L. K.; Wei, M.; Yap, P. H.; Zhou, X.; Zhao, H.; Yu, D.; Tsai, D. P.; Liu, A. Q. On-Chip Optical Detection of Viruses: A Review. *Adv. Photonics Res.* **2021**, *2*, No. 2000150.
(7) Soler, M.; Estevez, M. C.; Cardenosa-Rubio, M.; Astua, A.; Lechuga, L. M. How Nanophotonic Label-Free Biosensors Can Contribute to Rapid and Massive Diagnostics of Respiratory Virus Infections: COVID-19 Case. *ACS Sens.* **2020**, *5*, 2663−2678.
(8) Seo, G.; Lee, G.; Kim, M. J.; Baek, S.-H.; Choi, M.; Ku, K. B.; Lee, C.-S.; Jun, S.; Park, D.; Kim, H. G.; Kim, S.-J.; Lee, J.-O.; Kim, B. T.; Park, E. C.; Kim, S. I. Rapid Detection of COVID-19 Causative Virus (SARS-CoV-2) in Human Nasopharyngeal Swab Specimens Using Field-Effect Transistor-Based Biosensor. *ACS Nano* **2020**, *14*, 5135−5142.
(9) Poland, G. A.; Ovsyannikova, I. G.; Kennedy, R. B. SARS-CoV-2 immunity: review and applications to phase 3 vaccine candidates. *Lancet* **2020**, *396*, 1595−1606.
(10) Chen, H.; Guo, J.; Wang, C.; Luo, F.; Yu, X.; Zhang, W.; Li, J.; Zhao, D.; Xu, D.; Gong, Q.; Liao, J.; Yang, H.; Hou, W.; Zhang, Y. Clinical characteristics and intrauterine vertical transmission potential of COVID-19 infection in nine pregnant women: a retrospective review of medical records. *Lancet* **2020**, *395*, 809−815.
(11) Wiersinga, W. J.; Rhodes, A.; Cheng, A. C.; Peacock, S. J.; Prescott, H. C. Pathophysiology, Transmission, Diagnosis, and Treatment of Coronavirus Disease 2019 (COVID-19): A Review. *JAMA* **2020**, *324*, 782−793.
(12) Harvey, W. T.; Carabelli, A. M.; Jackson, B.; Gupta, R. K.; Thomson, E. C.; Harrison, E. M.; Ludden, C.; Reeve, R.; Rambaut, A.; Peacock, S. J.; Robertson, D. L. Consortium, C.-G. U. SARS-CoV-2 variants, spike mutations and immune escape. *Nat. Rev. Microbiol.* **2021**, *19*, 409−424.
(13) Grubaugh, N. D.; Hanage, W. P.; Rasmussen, A. L. Making sense of mutation: what D614G means for the Covid-19 pandemic remains unclear. *Cell* **2020**, *182*, 794−795.
(14) Ymeti, A.; Greve, J.; Lambeck, P. V.; Wink, T.; van, H.; Beumer; Wijn, R. R.; Heideman, R. G.; Subramaniam, V.; Kanger, J. S. Fast, Ultrasensitive Virus Detection Using a Young Interferometer Sensor. *Nano Lett.* **2007**, *7*, 394−397.
(15) Leong, J.-A.; Garapin, A.-C.; Jackson, N.; Fanshier, L.; Levinson, W.; Bishop, J. M. Virus-Specific Ribonucleic Acid in Cells Producing Rous Sarcoma Virus: Detection and Characterization. *J. Virol.* **1972**, *9*, 891−902.
(16) Edwards, M. L.; Cooper, J. I. Plant virus detection using a new form of indirect ELISA. *J. Virol. Methods* **1985**, *11*, 309−319.
(17) Draz, M. S.; Vasan, A.; Muthupandian, A.; Kanakasabapathy, M. K.; Thirumalaraju, P.; Sreeram, A.; Krishnakumar, S.; Yogesh, V.; Lin, W.; Yu, X. G.; Chung, R. T.; Shafiee, H. Virus detection using nanoparticles and deep neural network−enabled smartphone system. *Sci. Adv.* **2020**, *6*, No. eabd5354.
(18) Popovic, M.; Sarngadharan, M. G.; Read, E.; Gallo, R. C. Detection, isolation, and continuous production of cytopathic retroviruses (HTLV-III) from patients with AIDS and pre-AIDS. *Science* **1984**, *224*, 497.
(19) Yang, Y.; Liu, J.; Zhou, X. A CRISPR-based and post-amplification coupled SARS-CoV-2 detection with a portable evanescent wave biosensor. *Biosens. Bioelectron.* **2021**, *190*, No. 113418.
(20) Leland, D. S.; Ginocchio, C. C. Role of cell culture for virus detection in the age of technology. *Clin. Microbiol. Rev.* **2007**, *20*, 49−78.
(21) Pang, Y.; Song, H.; Kim, J. H.; Hou, X.; Cheng, W. Optical trapping of individual human immunodeficiency viruses in culture fluid reveals heterogeneity with single-molecule resolution. *Nat. Nanotechnol.* **2014**, *9*, 624−630.
(22) Shi, Y.; Xiong, S.; Chin, L. K.; Zhang, J.; Ser, W.; Wu, J.; Chen, T.; Yang, Z.; Hao, Y.; Liedberg, B.; Yap, P. H.; Tsai, D. P.; Qiu, C.-W.; Liu, A. Q. Nanometer-precision linear sorting with synchronized optofluidic dual barriers. *Sci. Adv.* **2018**, *4*, No. eaao0773.
(23) Ashkin, A.; Dziedzic, J. M. Optical trapping and manipulation of viruses and bacteria. *Science* **1987**, *235*, 1517−1520.
(24) Ashkin, A. History of optical trapping and manipulation of small-neutral particle, atoms, and molecules. *IEEE J. Sel. Top. Quantum Electron.* **2000**, *6*, 841−856.
(25) Shi, Y.; Zhao, H.; Nguyen, K. T.; Zhang, Y.; Chin, L. K.; Zhu, T.; Yu, Y.; Cai, H.; Yap, P. H.; Liu, P. Y.; Xiong, S.; Zhang, J.; Qiu, C.-W.; Chan, C. T.; Liu, A. Q. Nanophotonic Array-Induced Dynamic Behavior for Label-Free Shape-Selective Bacteria Sieving. *ACS Nano* **2019**, *13*, 12070−12080.
(26) Patolsky, F.; Zheng, G.; Hayden, O.; Lakadamyali, M.; Zhuang, X.; Lieber, C. M. Electrical detection of single viruses. *Proc. Natl. Acad. Sci. U.S.A.* **2004**, *101*, 14017.
(27) Gupta, A.; Akin, D.; Bashir, R. Single virus particle mass detection using microresonators with nanoscale thickness. *Appl. Phys. Lett.* **2004**, *84*, 1976−1978.
(28) Ozcelik, D.; Parks, J. W.; Wall, T. A.; Stott, M. A.; Cai, H.; Parks, J. W.; Hawkins, A. R.; Schmidt, H. Optofluidic wavelength division multiplexing for single-virus detection. *Proc. Natl. Acad. Sci. U.S.A.* **2015**, *112*, 12933.
(29) Black, J. A.; Ganjalizadeh, V.; Parks, J. W.; Schmidt, H. Multi-channel velocity multiplexing of single virus detection on an optofluidic chip. *Opt. Lett.* **2018**, *43*, 4425−4428.
(30) Mitra, A.; Deutsch, B.; Ignatovich, F.; Dykes, C.; Novotny, L. Nano-optofluidic Detection of Single Viruses and Nanoparticles. *ACS Nano* **2010**, *4*, 1305−1312.
(31) Wei, Q.; Qi, H.; Luo, W.; Tseng, D.; Ki, S. J.; Wan, Z.; Göröcs, Z.; Bentolila, L. A.; Wu, T.-T.; Sun, R.; Ozcan, A. Fluorescent Imaging of Single Nanoparticles and Viruses on a Smart Phone. *ACS Nano* **2013**, *7*, 9147−9155.
(32) Pokhrel, P.; Hu, C.; Mao, H. Detecting the Coronavirus (Covid-19). *ACS Sens.* **2020**, *5*, 2283−2296.
(33) Zanchetta, G.; Lanfranco, R.; Giavazzi, F.; Bellini, T.; Buscaglia, M. Emerging applications of label-free optical biosensors. *Nanophotonics* **2017**, *6*, 627−645.
(34) Shi, Y.; Zhao, H.; Chin, L. K.; Zhang, Y.; Yap, P. H.; Ser, W.; Qiu, C.-W.; Liu, A. Q. Optical Potential-Well Array for High-Selectivity, Massive Trapping and Sorting at Nanoscale. *Nano Lett.* **2020**, *20*, 5193−5200.
(35) Shi, Y. Z.; Xiong, S.; Zhang, Y.; Chin, L. K.; Chen, Y. Y.; Zhang, J. B.; Zhang, T. H.; Ser, W.; Larson, A.; Hoi, L. S.; Wu, J. H.; Chen, T. N.; Yang, Z. C.; Hao, Y. L.; Liedberg, B.; Yap, P. H.; Tsai, D. P.; Qiu, C. W.; Liu, A. Q.; et al. Sculpting nanoparticle dynamics for single-bacteria-level screening and direct binding-efficiency measurement. *Nat. Commun.* **2018**, *9*, No. 815.
(36) Shi, Y.; Zhu, T.; Zhang, T.; Mazzulla, A.; Tsai, D. P.; Ding, W.; Liu, A. Q.; Cipparrone, G.; Sáenz, J. J.; Qiu, C.-W. Chirality-assisted lateral momentum transfer for bidirectional enantioselective separation. *Light: Sci. Appl.* **2020**, *9*, No. 62.
(37) Zhu, T.; Shi, Y.; Ding, W.; Tsai, D. P.; Cao, T.; Liu, A. Q.; Nieto-Vesperinas, M.; Sáenz, J. J.; Wu, P. C.; Qiu, C.-W. Extraordinary Multipole Modes and Ultra-Enhanced Optical Lateral Force by Chirality. *Phys. Rev. Lett.* **2020**, *125*, No. 043901.
(38) Lion, T. Adenovirus Infections in Immunocompetent and Immunocompromised Patients. *Clin. Microbiol. Rev.* **2014**, *27*, 441.

https://doi.org/10.1021/acssensors.1c01350
ACS Sens. XXXX, XXX, XXX−XXX